

XAFS study on a pressure-induced superconductor Cs_3C_{60} under high pressure

Satoshi Fujiki,^a Yoshihiro Kubozono,^a Yasuhiro Takabayashi,^a Setsuo Kashino,^a and Shuichi Emura^b

^aOkayama University, Okayama 700-8530, Japan, ^bOsaka University, Osaka 567-0047, Japan.
Email: fuziki@cc.okayama-u.ac.jp

Cs K-edge XAFS of Cs_3C_{60} which is a pressure-induced superconductor were measured at 21 and 34 kbar by using a diamond anvil cell (DAC) in order to obtain the structural information under high pressure, and to clarify the origin of the pressure-induced superconductivity. The distances and the mean square displacements between the Cs and C atoms are consistent with those determined by X-ray powder diffraction. Consequently, the high-pressure XAFS can give the reliable structural-information on a fullerene superconductor under high pressure. We also show the procedure of the analysis of high-pressure XAFS with DAC in detail.

Keywords: Cs K-edge XAFS; pressure-induced superconductor; high pressure; DAC

1. Introduction

Palstra *et al.* (1995) reported that Cs_3C_{60} exhibited the superconducting critical temperature (T_c) of 40 K at 14.3 kbar. The T_c realized in Cs_3C_{60} is the highest one among fullerene superconductors. The T_c increased with an increase in pressure though Cs_3C_{60} was not a superconductor at 1 bar. Such a pressure-dependence was a contrast to that for the other superconductors, A_3C_{60} (A: Rb and K), which exhibited the decrease in T_c by applying pressure (Sparrn *et al.*, 1992). The crystal structure of Cs_3C_{60} was found to be of a body-centered orthorhombic (bco; *Immm*) as major phase and A15 (cubic; *Pm3m*) as minor phase (Yoshida *et al.*, 1998).

The behaviour of T_c observed in Cs_3C_{60} cannot be explained by the model that a band broadening by applying pressure reduces the density-of-state on the Fermi level, $N(\epsilon_F)$, and T_c as expected from the conventional BCS theory. One of the explanations for the behavior is that Cs_3C_{60} is a Mott-Hubbard insulator and transforms to an insulating state from a metallic state in the low temperature region at 1 bar. However, ESR showed that Cs_3C_{60} was metallic from 2 to 300 K at 1 bar (Yoshida *et al.*, 1998). Consequently, the origin of the pressure-induced superconductivity is not found at the present stage.

In the present study, we tried to study the structure of Cs_3C_{60} based on Cs K-edge XAFS under high pressure in order to approach to the origin of the pressure-induced superconductivity. We report the details of the experimental setup and the analysis for the high-pressure XAFS.

2. Experimental

2.1. Sample Preparation

The Cs_3C_{60} sample was prepared by a reaction of C_{60} with Cs metal in liquid NH_3 at -70°C for 1 h. After the complete reaction, NH_3 was pumped under 10^{-3} Torr at 100°C for 18 h and then 140

$^\circ\text{C}$ for 1 h. The Raman peak for the $A_g(2)$ mode of this sample was observed at 1446 cm^{-1} . The Rietveld analysis for the X-ray diffraction pattern showed that this sample was $\text{Cs}_{3.2(2)}\text{C}_{60}$; the fraction of the bco phase was larger than 99 %. The Cs atoms occupy two crystallographically independent sites of $4f$ and $4h$. If Cs atoms occupy completely these sites, the composition of sample is Cs_4C_{60} . The vacancies at $4f$ and $4h$ sites are randomly distributed in this sample.

2.2. XAFS measurement

Cs K-edge XAFS was measured at 21 and 34 kbar in a transmission mode with a Si(311) monochromator at BL01B1 of SPring-8. A Rh mirror was inserted to eliminate the harmonics. The energy resolution is less than 2 eV in Cs K-edge region (36000 eV). The sample was introduced into a diamond anvil cell (DAC) in a glove box to avoid the degradation of sample by air and water. The schematic representation of the DAC is shown in Fig. 1. The Cs_3C_{60} sample was placed in 300 μm hole of the gasket (Inconel, thickness 330 μm), and was covered by mineral oil to obtain the hydrostatic pressure. The sample was interposed by two diamond crystals as shown in Fig. 1. The X-ray beam was passed through the crystals as shown by an arrow (Fig. 1). The pressure was estimated according to the equation reported by Mao *et al.* (1978) with the fluorescence observed for the Ruby which was put on the sample. The DAC was set on a goniometer.

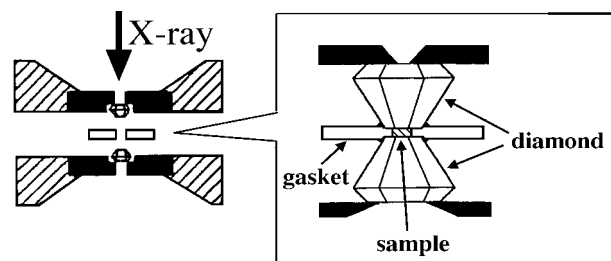


Figure 1
Experimental setup used for XAFS measurement under high pressure.

2.3. XAFS analyses

We measured several times the XAFS spectra of the Cs_3C_{60} sample at each pressure by rotating the DAC by small angles about the horizontal axis which is perpendicular to the X-ray beam; the rotation angle was within $\pm 0.2^\circ$. Some diffraction peaks from diamond were observed in the XAFS spectra, as is shown in Fig. 2(a). The energy E at which the diffraction peak was observed shifted by rotating the DAC [Fig. 2(a)]. The spectrum was obtained by replacing the μ in the E -regions with diffraction peaks with that in the corresponding E regions without diffraction peaks at the other rotation

The XAFS oscillation $\chi(k)$ was extracted from the observed XAFS spectrum by eliminating the background using Victoreen's formula, cubic spline method and McMaster coefficients (McMaster *et al.*, 1969). The threshold energy E_0 was determined from the inflection point of X-ray absorption edge. The radial structure function $\Phi(r)$ in the real space (r -space) was obtained by a Fourier transform of the $k^3\chi(k)$ in momentum space (k -space) of photoelectron. The structural parameters were obtained by a least-squares fitting to the $\chi(k)$ derived by an inverse-Fourier transform of $\Phi(r)$ with XAFS formula within the framework of the harmonic approximation (Ishii, 1991). The theoretical values reported by McKale (1988) were used for the phase shifts of the

absorbing and scattering atoms, and backscattering amplitudes of the scattering atoms. The FEFF code (Rehr *et al.*, 1991) was also applied to the XAFS analysis at 21 kbar. All analyses were performed by using programs XAFS 93 and MBF93 [McKale] and FBF95 [FBFF] developed by Maeda.

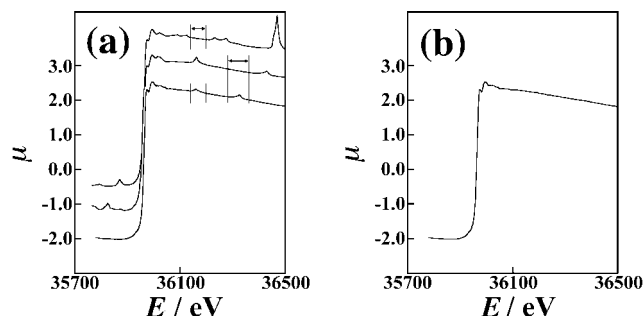


Figure 2
 (a) XAFS spectra obtained at three different rotation angles of the DAC, showing that the E -region for the diffraction peaks depends on the rotation angle. (b) An illustration of the XAFS spectrum used for the analysis. The spectrum was produced by replacing the μ with the diffraction peak in the bottom spectrum with non-diffraction peak region in the other spectra (top and middle) shown in (a). The replaced regions are shown by arrows. Though in this procedure the magnitude of μ hardly changed because of the very small rotation, the slight difference in the magnitude was corrected so that each μ fits.

3. Results and Discussion

The $k^3\chi(k)$ at 21 kbar is shown in Fig. 3(a). The imaginary part of $\Phi(r)$ obtained by a Fourier transform of $k^3\chi(k)$ in the k -region from 2.0 to 9.0 \AA^{-1} at 21 kbar exhibits a pronounced peak at 2.6 \AA [Fig. 3(b)]. The peak can be assigned to the Cs-C scattering. The Rietveld analysis of the X-ray powder diffraction at 21 kbar shows a distribution in the Cs-C distances, $r_{\text{Cs-C}}$, from 3.29 to 3.74 \AA for Cs atom at 4*f* and from 3.29 to 3.78 \AA for Cs atom at 4*h* (Kubozono *et al.*, 1999). Two five-membered rings and two six-membered rings of the C_{60} molecules face to the Cs atoms. The coordination of the C_{60} molecule around Cs atom at 4*h* is shown in Fig. 4. The Cs-C distributions for both Cs atoms were substantially the same. The $r_{\text{Cs-C}}$ were divided into two shells based on the Cs-C distribution because the Cs-C distances are distributed in the narrow region according to the normal statistics except for four Cs-C. The coordination number, N , and the average value of $r_{\text{Cs-C}}$, $\langle r_{\text{Cs-C}} \rangle$, are 18 and 3.46 \AA , respectively, for the first shell; $N = 4$ and $\langle r_{\text{Cs-C}} \rangle = 3.76 \text{\AA}$ for the second shell.

On the basis of this model, the two-shell-fitting was performed for the $\chi(k)$ obtained by the inverse-Fourier transform of the $\Phi(r)$ from 1.88 to 3.28 \AA . The N were fixed to the above values, and the S values were also fixed to 1.0 in order to avoid the correlation of parameters [S , N and $\sigma(2)$]. The distance between the Cs and C atoms in the first shell, $r_{\text{Cs-C}(1)}$, and the mean square displacement, $\sigma_1(2)$, were 3.38(3) \AA and 0.022(6) \AA^2 , respectively, while the Cs-C distance, $r_{\text{Cs-C}(2)}$, in the second shell and the mean square displacement, $\sigma_2(2)$, were 3.63(5) \AA and 0.007(7) \AA^2 , respectively. The relatively large $\sigma_1(2)$ can be well explained by the distribution in Cs-C, i.e., static disorder. The shift from E_0 (ΔE) and mean free path (λ) of photoelectron were parameterized. The ΔE and λ were -5 eV and $\lambda = 0.6k \text{\AA}$, respectively. The final R -factor was 0.06. Though the one-shell fitting was also performed in this analysis, the experimental $\chi(k)$ could not be reproduced; the R -factor was more than 0.20.

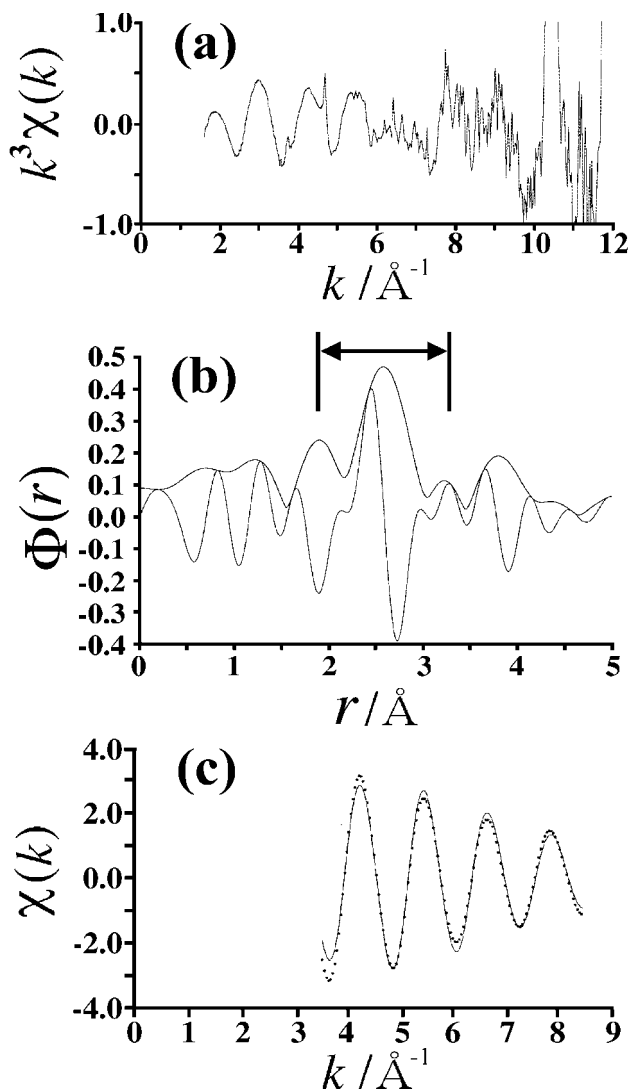


Figure 3
 (a) $k^3\chi(k)$ and (b) $\Phi(r)$ at 21 kbar. The thick and thin lines refer to the magnitude and imaginary part of $\Phi(r)$. The range of Fourier transformation is shown by an arrow. (a) The closed circles and solid line refer to the experimental XAFS obtained by an inverse-Fourier transformation of $\Phi(r)$ at 21 kbar.

Further, the analysis with FEFF code was performed in order to check the validity of the structural parameters determined with McKale's values. The $r_{\text{Cs-C}(1)}$ and $r_{\text{Cs-C}(2)}$, were determined by FEFF code to be 3.38(4) and 3.64(5) \AA , respectively, and the $\sigma_1(2)$ and $\sigma_2(2)$ were 0.027(7) and 0.007(8) \AA^2 , respectively. These are consistent with those determined with McKale's values within the esd. The observed $\chi(k)$ and calculated one with the final parameters (McKale) are shown in Fig. 3(c). Both $r_{\text{Cs-C}(1)}$ and $r_{\text{Cs-C}(2)}$ were consistent with the $\langle r_{\text{Cs-C}} \rangle$ in the first and the second shells, respectively, estimated by the Rietveld analysis (Kubozono *et al.*, 1999). The result demonstrates that the high-pressure XAFS of fullerene superconductor with the DAC can give the reliable structural-information.

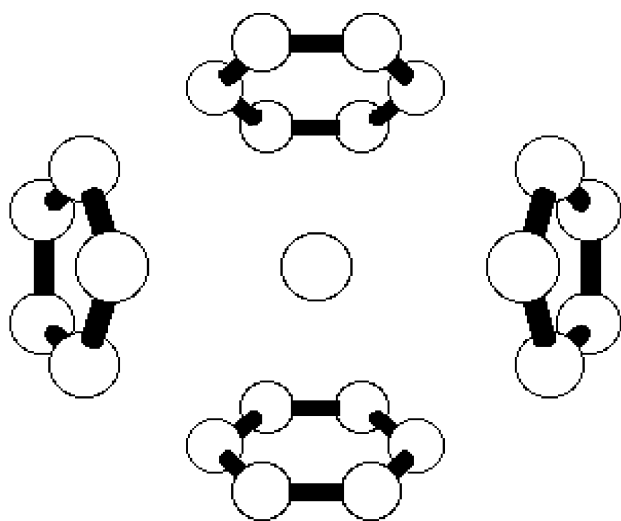


Figure 4

A view of the coordination of Cs atom (4h) to the two neighboring six-membered rings and two five-membered rings from the nearest C_{60} molecules.

The imaginary part of $\Phi(r)$ obtained from $k^3\chi(k)$ from 2.5 to 8.0 \AA^{-1} at 34 kbar exhibits a pronounced peak at 2.49 \AA . The $\chi(k)$ was obtained by the inverse-Fourier transform of the $\Phi(r)$ from 1.90 to 3.37 \AA^{-1} . The $r_{Cs-C(1)}$ and $r_{Cs-C(2)}$ were determined to be $3.38(3)$ and $3.65(7) \text{ \AA}$, respectively; in this analysis, the final R -factor was 0.12. The N were fixed to 20 and 2 on the basis of the results of the Rietveld analysis for the X-ray powder diffraction of Cs_3C_{60} at 34 kbar. These values were almost the same as the $\langle r_{Cs-C} \rangle$ by the Rietveld analysis ($\langle r_{Cs-C} \rangle = 3.32 \text{ \AA}$ for the first shell and $\langle r_{Cs-C} \rangle = 3.71 \text{ \AA}$ for the second shell). The $\sigma_1(2)$ and $\sigma_2(2)$ were $0.022(6)$ and $0.001(9) \text{ \AA}^2$, respectively. Though the $\sigma_1(2)$ was the same at both pressures, the $\sigma_2(2)$ at 34 kbar was smaller than that at 21 kbar which may be attributed to the suppression of thermal fluctuation at high pressure. Furthermore, we analyzed the XAFS at 34 kbar under the N of 18 and 4 in the same manner as the analysis at 21 kbar. The $r_{Cs-C(1)}$ and $r_{Cs-C(2)}$ were determined to be $3.39(3)$ and $3.66(5) \text{ \AA}$, respectively, which are consistent with those determined under the N of 20 and 2 within the esd. The $\sigma_1(2)$ and $\sigma_2(2)$ were $0.018(4)$ and $0.003(7) \text{ \AA}^2$, respectively, which are also consistent with those under $N = 20$ and 2. The suppression of thermal fluctuation by applying pressure is also found in this analysis.

This work was achieved under the proposals of (1998A0048-CX-np of SPring-8) and (98G289 of KEK-PF), and was supported by a Grant-in-aid (12640557) from the Ministry of Education, Science, Sports, and Culture, Japan.

References

- Ishii, T. (1992). *J. Phys. Condens. Matter*, **4**, 8029-8034.
 Kubozono, Y., Fujiki, S., Takabayashi, Y., Yoshida, Y., Kashino, S., Ishii, K., Fujiwara, A. & Suematsu, H. *Electronic of Novel Materials - Science and Technology of Molecular Nanostructures*, edited by Kuzmany, K., Fink, J., Mehring, M. & Roth, S. (1999). pp. 69-72.
 Mao, H. K., Bell, P. M., Shaner, J. W. & Sternberg, D. J. (1978). *J. Appl. Phys.* **49**, 3276-3283.
 McKale, A. G., Veal, B. W., Paulikas, A. P., Chan, S.-K. & Knapp, G. S. (1988). *J. Am. Chem. Soc.* **110**, 3763-3768.
 McMaster, W. H., Kerr, N., Grande, D., Mallet, J. H. & Hubell, J. H. (1969). *Combination of x-ray cross sections*, National Technical Information Service, Springfield.
 Palstra, T. T. M., Zhou, O., Iwasa, Y., Sulewski, P. E., Fleming, R. M. & Zegarski, O. (1995). *Solid State Commun.* **93**, 327-330.
 Rehr, J. J., Mustre de Leon, J., Zabinsky, S. I. & Albers, R. C. (1991). *J. Am. Chem. Soc.* **113**, 5135-5140.
 Sparr, G., Thompson, J. D., Whetten, R. L., Huang, S.-M., Kaner, R. B., Diederich, F., Gruner, G. & Holczer, K. (1992). *Phys. Rev. Lett.* **68**, 1228-1231.
 Yoshida, Y., Kubozono, Y., Kashino, S. & Murakami, Y. (1998). *Chem. Phys. Lett.* **291**, 31-36.